processes

MDPI

Article

Decomposition Mechanism and Calcination Properties of Small-Sized Limestone at Steelmaking Temperature

Kaixuan Zhang, Shuhuan Wang, Chenxiao Li *, Huakang Sun and Yun Zhang

Tangshan Key Laboratory of Special Metallurgy and Material Manufacture, North China University of Science and Technology, Tangshan 063210, China
* Correspondence: lichenxiao34@163.com; Tel.: +86-188-1159-0603

Abstract: Limestone with a particle size of less than 5 mm was rapidly calcined in a high-temperature resistance furnace at 1623 K to simulate the conditions of rapid calcination of limestone at ultra-high temperature in a converter. In this study, the decomposition mechanism and calcination characteristics of small-sized limestone at steelmaking temperature were investigated. The study shows that the shrinking sphere or cylinder models with phase boundary reaction were found to be the best representation of limestone kinetic data, and the mechanism function equation is $G(\alpha) = 1 - (1 - \alpha)^n$, n = 1/2 or 1/3. Limestone particles with a size of 0.18–1.0 mm can be quickly calcined to obtain a typical active lime microstructure and a high activity of more than 350 mL, which is the preferred limestone particle size range in the steelmaking process in which limestone powder is injected into the converter.

Keywords: high-temperature rapid calcination; small-sized limestone; decomposition mechanism; microstructure; lime activity

Citation: Zhang, K.; Wang, S.; Li, C.; Sun, H.; Zhang, Y. Decomposition Mechanism and Calcination Properties of Small-Sized Limestone at Steelmaking Temperature. *Processes* **2023**, *11*, 1008. https://doi.org/10.3390/pr11041008

Academic Editor: Blaž Likozar

Received: 3 March 2023
Revised: 19 March 2023
Accepted: 20 March 2023
Published: 27 March 2023

1. Introduction

Since China announced, in September 2020, that it would achieve "carbon peak" in 2030 and "carbon neutrality" in 2060, the iron and steel industry has actively taken measures to save energy and reduce consumption and emissions, eliminate backwardness, and increase environmentally friendly production, etc. The includes the application of the "slag-making steel with limestone instead of lime in converter" process to achieve energy savings, emission reduction, and efficient smelting in steel production, thus putting the low-carbon transformation into practice [1–5].

In this process, the limestone is instantly calcined in a high-temperature environment above 1623 K. The calcination process differs significantly from the process of slowly heating in a lime kiln for calcination. Therefore, clarification of the decomposition mechanism and physicochemical properties of limestone under rapid heating is one of the most important issues in this process. The high-temperature calcination of limestone has been studied by many researchers [6–10]. Hu Bin et al. [11] conducted a high-temperature calcination test at 1623–1773 K for limestone particles with an average particle size of 17.5 mm and found that the thermal decomposition reaction of limestone by kinetic analysis was consistent with the model of random nucleation and the subsequent growth model. Ghiasi M. et al. [12] performed isothermal kinetic analysis on limestone particles with a particle size of 0.885–10.763 mm and found that the modified shrinkage core model could better characterize the kinetic data. Cai Jinlin et al. [13] rapidly calcined large pieces of limestone with particle sizes of 12.5–15 mm at 1723 K and determined the relationship between the physical and chemical properties, activity, and microstructural changes of lime under these conditions. Li Chenxiao et al. [14] investigated the influence of micromorphology on the physical parameters and activity of limestones after calcination by selecting limestones from three producing areas and found that, at the same calcination temperature and time, the porosity and activity of lime obtained after calcination were higher as the micro-grain size of the limestone increased. Wang L et al. [15] found that when limestones

were calcined at 1623–1823 K, with the increase of calcination temperature, the pore size of lime became larger, the number of micropores decreased accordingly, and the maximum activity of the lime also showed a decreasing trend.

However, there are few studies on the calcination of small-sized limestone at high temperature. Continuous injection of limestone powder into the converter is used for slag steelmaking to optimize the process of direct steelmaking with limestone in the converter and solve the problems of low decomposition rate and difficult slag melting when massive limestone with an average particle size of about 20 mm is added to the converter in practice. Fine limestone powder particles are directly injected into the converter through high-pressure gas for smelting, greatly increasing the contact area and surface activity of limestone powder particles and liquid metal, while generating a strong stirring effect on the molten pool, creating good thermodynamic and dynamic conditions for smelting, thereby improving the slag-forming effect and dephosphorization rate. The rapid calcination process of small-sized limestone at high temperature must be included in the new process. Therefore, it is of great significance to study the decomposition mechanism and calcination properties of small-sized limestone at steelmaking temperature.

In this paper, the conversion degree changes of limestone with particle size less than 5 mm were examined when calcined at 1623 K. The decomposition mechanism of limestone under these conditions is systematically analyzed and the most probable mechanism function of its thermal analysis dynamics is determined by the pattern-matching method. Calcination properties, including the microstructure and activity of small-sized limestones, are studied. Then, the suitable limestone particle size range for injection is determined to provide guidance for the steelmaking process of injecting limestone powder into the converter.

2. Materials and Methods

2.1. Physical and Chemical Properties of Limestone

The selected limestone comes from the limestone supply area of a steel company, the chemical composition of which is shown in Table 1. The content of $CaCO_3$ is nearly 99%, and the limestone contains only a small amount of MgO and a very low content of SiO_2 and S, which makes it a high-quality metallurgical lime.

Table 1. Chemical composition of limestone (%).

CaO	MgO	SiO_2	S	Loss in Ignition
≤0.003	≤0.03	0.1~0.2	≤0.006	≤0.007

Figure 1 shows the microstructure of the limestone under a scanning electron microscope. The grain size of $CaCO_3$ is small, about 2 μm, and the dislocation is large. During calcination, the CO_2 produced during decomposition can escape from the numerous fine grains on the surface and form a large number of micropores, which improve the specific surface area and porosity of the limestone.

Large limestones with a diameter of about 100 mm were gradually placed into jaw crushers with different particle sizes for multiple crushing and then poured into standard sieves for screening to obtain seven groups of limestone particles with different particle sizes: 3.0–5.0 mm, 2.0–3.0 mm, 1.0–2.0 mm, 0.68–1.0 mm, 018–0.68 mm, 0.074–0.18 mm, and below 0.074 mm. After ultrasonic cleaning, the sieved particles were dried to a constant weight at 393 K, numbered accordingly, packed into bags, and placed in a drying oven for use.

2.2. Test Equipment and Methods

The experimental apparatus for calcining limestone is shown in Figure 2. It consists of a vertical high-temperature resistance furnace, an electronic balance (measurement accuracy ± 0.0001 g), and a computer. The calcination temperature in the resistance furnace was 1623 K. The electronic balance on the top of the resistor furnace was connected to the computer to record the mass change of the limestone sample during the decomposition

experiment. Before the experiment, the empty quartz crucible was hung under the balance with a high-temperature resistance wire, and the balance was cleared. After the furnace temperature rose to the specified temperature, 2 g samples were placed in the crucible and the calcination test began. The weight loss of the limestone was recorded by the computer in real time, and the decomposition conversion degree of the limestone samples was calculated based on the real-time quality data. After calcination for a specified time, the reacted lime was quickly removed and cooled to room temperature in a metal dish. After the samples were photographed by a camera, the samples were stored for the determination of lime activity by the acid–base synthesis method and the observation of the microstructure of the calcined limestone by a scanning electron microscope. In order to reduce test error, each group of tests was repeated 3 times to obtain the average value.

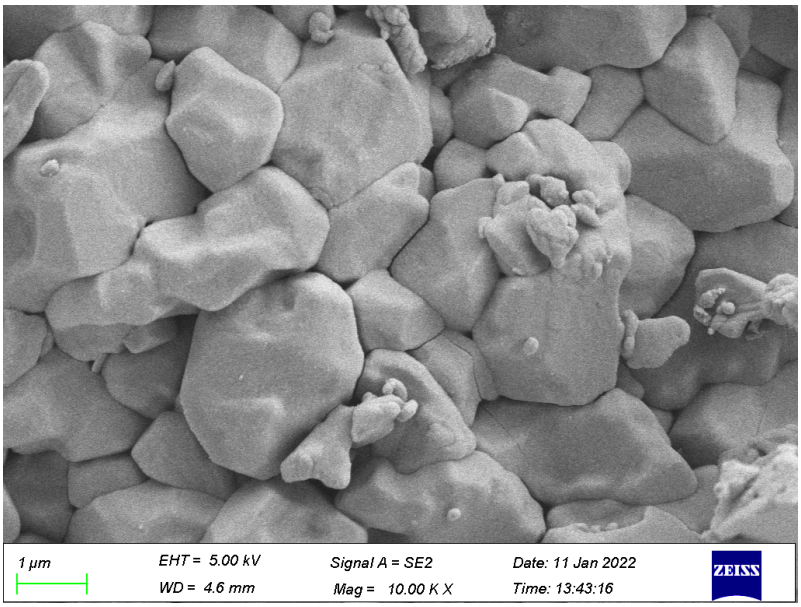

Figure 1. The microstructure of limestone.

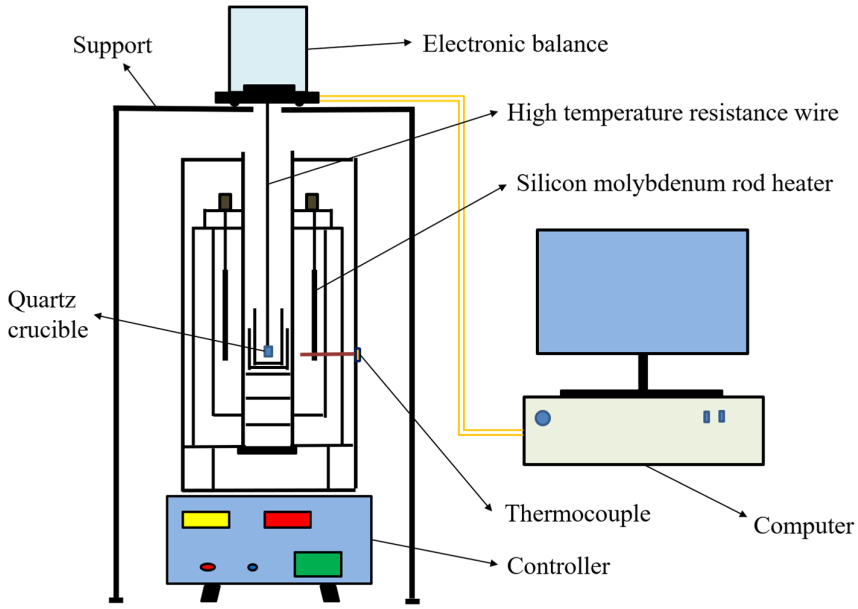

Figure 2. Schematic diagram of a high-temperature resistance furnace for calcination of limestone.

When calcining limestone at 1623 K, $CaCO_3$ rapidly absorbs a large amount of heat and decomposes to release the CO_2 gas. The recorded mass of the test process is the change of

limestone mass with time, and the conversion degree of limestone decomposition reaction is indirectly expressed by the weight loss of limestone. The decomposition conversion degree α of $CaCO_3$ is calculated according to Equation (1).

$$\alpha = \frac{w_0 - w_t}{w_0 - w_x} \times 100\% \quad (1)$$

In Equation (1):
w_0—Initial quality of the limestone sample, g;
w_t—Mass of limestone sample at reaction time t, g;
w_x—The remaining mass of the sample when the reaction is complete, g.

Since calcination of limestone was performed at a constant temperature of 1623 K, the possible mechanism function $G(\alpha)$ of its thermal analysis kinetics was determined by the isothermal method. According to the kinetic equation of the isothermal method (Equation (2)) [16]:

$$G(\alpha) = \int_0^\alpha \frac{d\alpha}{f(\alpha)} = kt \quad (2)$$

In Equation (2):
$G(\alpha)$—Reaction mechanism function in the integral form;
$f(\alpha)$—Reaction mechanism function in differential form;
α—decomposition conversion degree of limestone;
k—Chemical reaction rate constant, s^{-1}.

The pattern-matching method was applied, and using the α-t data of limestone particles with different particle sizes, different mechanism functions were used for linear fitting in Equation (2), and the function that best reflected the linearity was the most likely mechanism function of the reaction. The 30 kinetic reaction mechanisms and functional equations commonly used for solid reactions are listed in Table 2 [16].

Table 2. Thirty reaction mechanisms and functions of kinetics.

Function Serial Number	Function Name	Mechanism	Mechanism Function in the Integral Form: G(α)
1	The principle of parabola	One-dimensional diffusion	α^2
2	The Valensi equation	Two-dimensional diffusion	$\alpha + (1-\alpha)\ln(1-\alpha)$
3	The Ginstling–Brounshtein equation	Three-dimensional diffusion, with cylindrical symmetry	$1 - 2\alpha/3 - (1-\alpha)^{2/3}$
4, 5	Jander equation	Three-dimensional diffusion, with spherical symmetry	$[1-(1-\alpha)^{1/3}]^n$ (n = 2,1/2)
6	Jander equation	Two-dimensional diffusion, n = 1/2	$[1-(1-\alpha)^{1/2}]^{1/2}$
7	Inverse Jander equation	Three-dimensional diffusion	$[(1+\alpha)^{1/3} - 1]^2$
8	The Zhuralev–Lesokin–Tempelman equation	Three-dimensional diffusion	$[(1-\alpha)^{1/3} - 1]^2$
9	Mample one-line rule, Level 1	Random nucleation and subsequent growth of the single core	$-\ln(1-\alpha)$
10–16	The Avranmi–Erofeev equation	Random nucleation and subsequent growth	$[-\ln(1-\alpha)]^n$ (n = 2/3, 1/2, 1/3, 4, 1/4, 2, 3)
17–20	Shrinking cylinder (area)	Phase boundary reaction, with cylindrical symmetry	$1-(1-\alpha)^n$ (n = 1/2, 3, 2, 4)
21, 22	Shrinking sphere (volume)	Phase boundary reaction, with spherical symmetry	$1-(1-\alpha)^n$ (n = 1/3, 1/4)
23–27	Power law	Phase boundary reaction	α^n (n = 1, 3/2, 1/2, 1/3, 1/4)
28	Second-order reaction	Chemical reaction	$(1-\alpha)^{-1}$
29	Reaction order	Chemical reaction	$(1-\alpha)^{-1} - 1$
30	2/3 order reaction	Chemical reaction	$(1-\alpha)^{-1/2}$

3. Test Results and Discussion

3.1. The Decomposition Process of Limestone Particles Calcined at High Temperature

3.1.1. Thermodynamic Analysis of Pyrolysis of Limestone Particles

The reaction equation of $CaCO_3$ pyrolysis is Equation (3) [17]:

$$CaCO_3 = CaO + CO_2 \quad \Delta_r G_m^{\Theta} = 170577 - 149019T,\ J{\cdot}mol^{-1} \tag{3}$$

From the Van't Hoff equation (Equation (4)), it is known that:

$$\Delta_r G_m^{\Theta} = -RT \ln p_{CO_2(CaCO_3)} \tag{4}$$

In the equation, $p_{CO_2(CaCO_3)}$ is the decomposition pressure of $CaCO_3$. The greater the decomposition pressure, the greater $-\Delta_r G_m^{\Theta}$ and the easier the decomposition of $CaCO_3$, so the decomposition pressure can be used as a measure of the decomposition tendency of $CaCO_3$. When the decomposition pressure reaches the total ambient pressure, $CaCO_3$ decomposes violently, and the decomposition temperature at this time is called the boiling temperature, which is also the actual decomposition temperature of $CaCO_3$.

The relationship between the decomposition pressure of $CaCO_3$ and the temperature is shown in Equation (5) [17]:

$$\lg p_{CO_2(CaCO_3)} = -8908/T + 7.53 \tag{5}$$

Under normal pressure (100 kPa), the boiling temperature of limestone calculated by the above formula is 1183 K, and in the process of slag-making steelmaking by spraying limestone powder in the converter, the limestone is instantly injected into the high-temperature environment of about 1623 K. The decomposition pressure of $CaCO_3$ at this temperature is up to 10,964 kPa, which is approximately 109 times the decomposition pressure at 1183 K, and $CaCO_3$ decomposes even faster.

The decomposition pressure of limestone with small particle size depends on the state of the particles before and after decomposition, especially on the particle radius, compared to limestone with large particle size. The smaller the particle size of limestone, the larger its surface area, and the greater its chemical potential; therefore, the decomposition pressure changes. Considering the effect of limestone particle size, the decomposition pressure can be expressed as Equation (6) [18]:

$$RT\ln p_{CO_2(CaCO_3)} = RT\ln p^{V}_{CO_2(CaCO_3)} + \left(\frac{2\sigma_{CaCO_3} V_{CaCO_3}}{r_{CaCO_3}} - \frac{2\sigma_{CaO} V_{CaO}}{r_{CaO}}\right) \tag{6}$$

In Equation (6):

$p^{V}_{CO_2(CaCO_3)}$—Decomposition pressure of $CaCO_3$ without consideration of particle size or surface energy;

σ_{CaCO3}, σ_{CaO}—The surface energies of $CaCO_3$ and CaO, $J{\cdot}m^{-2}$;

V_{CaCO3}, V_{CaO}—The partial molar volumes of $CaCO_3$ and CaO, $m^3{\cdot}mol^{-1}$;

r_{CaCO3}, r_{CaO}—The particle radius of $CaCO_3$ and CaO, m.

It can be seen from Equation (6) that with the decrease of limestone particle size, the decomposition pressure increases, and the increase is related to $\sigma V(\frac{1}{r_{CaCO_3}} - \frac{1}{r_{CaO}})$.

3.1.2. Kinetic Analysis of Pyrolysis of Limestone Particles

Using the data on limestone calcination over time obtained from the test, the 30 kinetic reaction mechanism functions in Table 2 were substituted into Equation (2) to be linearly fitted using the pattern-matching method, and the mechanism functions with the best fitting results were selected. The optimal fitting results for limestone with different particle sizes are shown in Table 3.

Table 3. The optimal fitting results of kinetic mechanism functions for limestone with different particle sizes.

Grain Size/mm	Function Serial Number of Optimal Fitting	Function Name	Mechanism	Goodness of Fit
3.0–5.0	21	Shrinking sphere (volume)	Phase boundary reaction, with spherical symmetry, n = 1/3	0.9896
2.0–3.0				0.9920
1.0–2.0				0.9890
0.68–1.0				0.9944
0.18–0.68	17	Shrinking cylinder (area)	Phase boundary reaction, with cylindrical symmetry, n = 1/2	0.9924
0.074–0.18				0.9918
less than 0.074				0.9959

When the limestone particle size is between 0.18–5.0 mm, the most probable mechanism function is function no. 21, and the function mechanism is the shrinking sphere model with phase boundary reaction, n = 1/3, and the function integral equation is $G(\alpha) = 1 - (1 - \alpha)^{1/3}$.

When the limestone particle size is less than 0.18 mm, the most probable mechanism function is No. 17 function, and the function mechanism is the shrinking cylinder model with phase boundary reaction, n = 1/2, and the function integral equation is $G(\alpha) = 1 - (1 - \alpha)^{1/2}$.

The decomposition reaction of $CaCO_3$ starts at the surface of the limestone and moves layer by layer to the center of the particle, and there is an obvious interface between the reactant and the product [19]. There are five links involved in the decomposition process, including two heat transfer processes, one chemical reaction, and two mass transfer processes:

1. Heat spreads on the surface of limestone particles;
2. Heat is transferred from the particle surface to the decomposition surface;
3. $CaCO_3$ decomposes and produces CaO and CO_2 gas at the solid–solid reaction interface;
4. CO_2 gas diffuses through the CaO layer to the surface;
5. The CO_2 on the surface diffuses into the surrounding airflow medium.

The limestone is divided into three layers during the calcination process: the overburned layer, the reaction layer, and the unreacted layer, as shown in Figure 3.

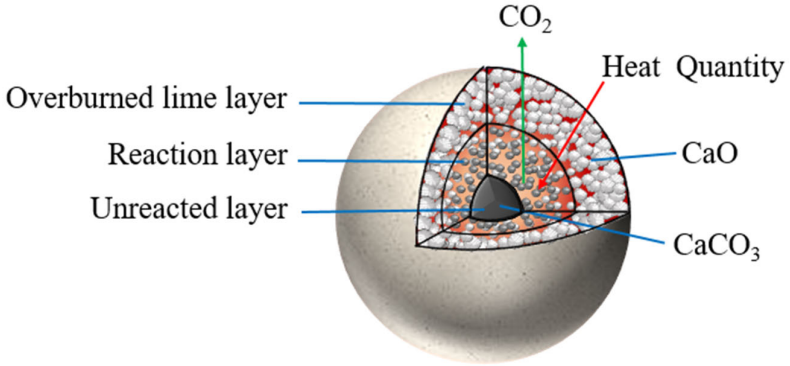

Figure 3. Schematic diagram of the decomposition of high-temperature calcined spherical calcium carbonate.

The decomposition of $CaCO_3$ exhibits the characteristics of a crystalline chemical transformation. The $Ca^{2+} \cdot O^{2-}$ group formed by decomposition is only very slightly soluble in the old phase of $CaCO_3$, so that a supersaturated state can easily form, from which the new phase nucleus of CaO is then formed by nucleation and growth. At high temperatures, the supersaturation of CaO in the old phase $CaCO_3$ is very large, which obviously shortens the induction period of the CaO phase nucleus, so that the reaction reaches a very high rate at the beginning. The new CaO is in a metastable state, with small grains and a large specific surface area. A large number of pores between the grains are conducive to the internal diffusion of CO_2 and accelerates the advancement of the reaction layer into the particles.

The CaO grains grow gradually with the extension of the calcination time. Grain growth is essentially a process of grain boundary displacement. According to the relationship between grain boundary migration rate and temperature (Equation (7)) [20]:

$$G = G_0 \exp\left(-\frac{Q_G}{RT}\right) \quad (7)$$

In Equation (7), G is the grain boundary migration rate, G_0 is a constant, and Q_G is the activation energy of grain boundary migration. The grain boundary migration rate increases exponentially with the temperature. Under the high temperature of 1623 K, CaO crystals first develop and decompose on the particle surface and grow rapidly, and the pores shrink, resulting in the formation of a dense overburned layer that thickens layer by layer to the internal depth of the particles. The overburned layer impedes the outward escape of CO_2 products, leading to an increase in the internal CO_2 concentration and limiting the decomposition reaction.

At the same time, with the increase of CaO product, the rate of heat transfer to the reaction interface decreases, because the thermal conductivity of lime is about 0.8 W/(m·K), which is slightly lower than that of limestone (0.2–1.35 W/(m·K)). The decomposition rate of limestone is hindered, which leads to a reduction in the growth rate of the reaction layer.

3.2. Conversion Degree of Small-Sized Limestones Calcined Rapidly at High Temperature

Figure 4 shows the conversion degree of calcined limestone particles with different particle sizes as a function of time at 1623 K. The reaction rate of high-temperature decomposition of limestone particles with different particle sizes first increases and then decreases until the reaction is completed and the decomposition rate becomes 0 when the limestone conversion is 100%. The time-dependent curves of the conversion degree of limestone particles with a particle size of 0.18–0.68 mm and 0.68–1.0 mm essentially overlapped, and both first reached 100% at about 100 s, which completed the decomposition reaction. The limestone particles with a particle size less than 0.074 mm were rapidly calcined due to their small size at the initial stage of calcination, but then strong bonds occurred to prevent the CO_2 from diffusing outward, which slowed the reaction rate and significantly reduced the conversion degree, and the reaction was completed only after about 150 s of calcination.

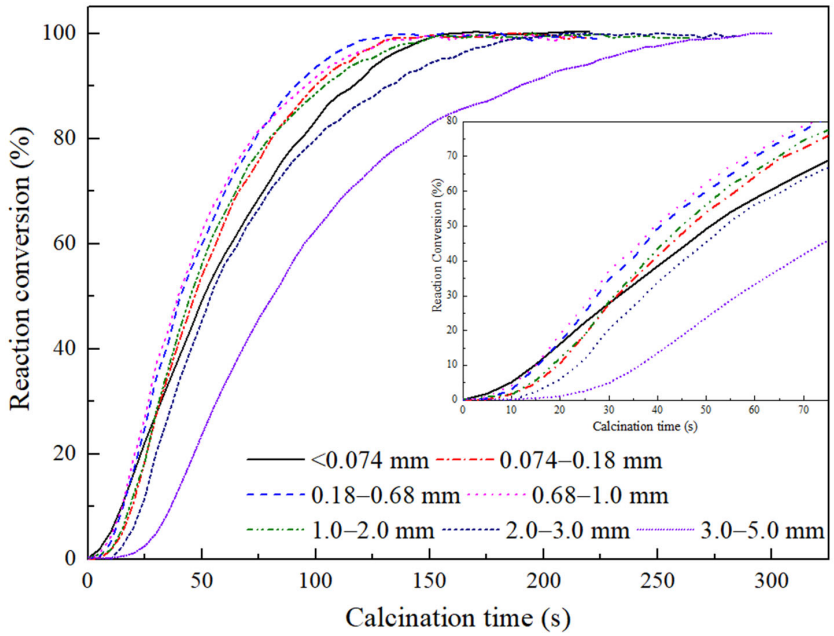

Figure 4. The conversion degree of limestone with different particle sizes with calcination time at 1623 K.

The conversion degrees of limestone with different particle sizes at a calcination time of 60 s were selected for comparison, as shown in Figure 5. Limestone particles with a particle size of 1.0–5.0 mm showed a significant increase in the conversion degree with decreasing particle size, and the time required to complete the decomposition reaction was greatly reduced. However, for limestone particles with particle sizes of 0.074–0.18 mm and below 0.074 mm, the conversion degree decreased with decreasing particle size, and the time required to complete decomposition increased.

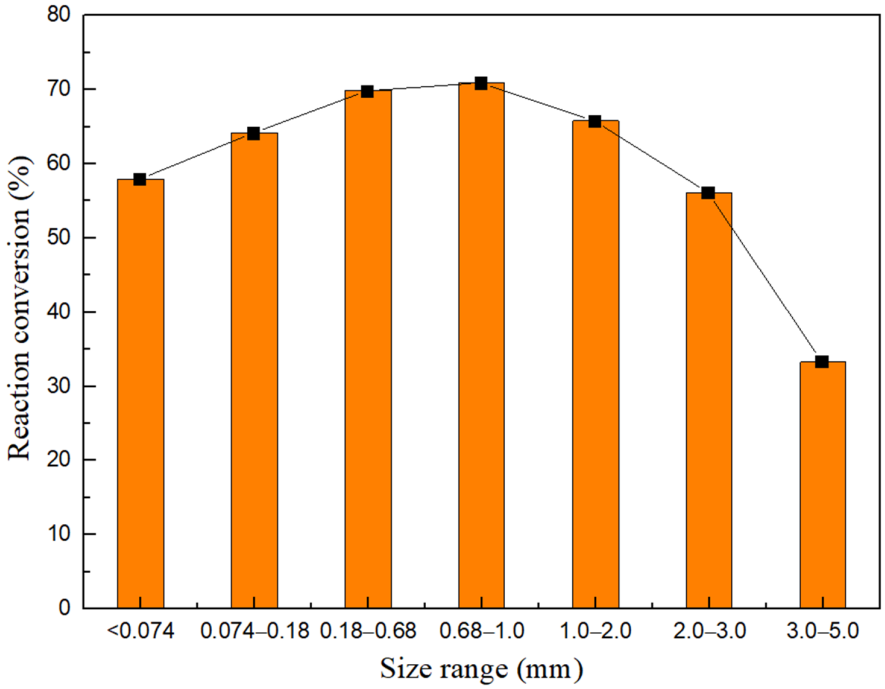

Figure 5. Conversion of limestone with different particle sizes during calcination for 60 s.

It can be seen that particle size is one of the most important influencing factors in high-temperature rapid calcination of limestone. Small-sized limestones have a high conversion degree, which can significantly accelerate the decomposition reaction, but due to the bonding phenomenon, a smaller particle size is not necessarily better. Limestone particles with a particle size of 0.18–1.0 mm have the fastest decomposition reaction and the shortest reaction completion time.

3.3. Microstructure of Small-Sized Limestones Calcined Rapidly at High Temperature

According to the results of the conversion degree experiments, three groups of limestone particles with particle sizes of 3.0–5.0 mm, 0.68–1.0 mm, and below 0.074 mm were selected to analyze the morphological changes after rapid calcination at 1623 K until no significant change in mass occurred, as shown in Figure 6. Figure 6a–c shows the original morphology of limestone particles before calcination; Figure 6d–f shows the macroscopic morphology of limestone particles after calcination; and Figure 6g–i shows the microscopic morphology of the surface of limestone particles after calcination.

For limestone particles with particle sizes of 3.0–5.0 mm and 0.68–1.0 mm, significant cracking noise could be heard in the early stage of calcination. Figure 6d,e,g,h show that numerous cracks were visible on the surface of the particles after calcination was completed. As the particle size decreased, the width of the cracks decreased and the number increased, and the wide and long cracks were converted into a large number of narrow cracks. This is because after the limestone particles were directly placed in a high-temperature environment of 1623 K, the surface of the limestone heated rapidly and formed a huge temperature difference with the interior, resulting in thermal stresses. Together with the internal stresses generated by CO_2, the sum of the two stresses exceeded the

maximum tensile stress of the limestone, resulting in cracks in the limestone surface [21,22]. The conversion degrees of limestone of different particle sizes in Figure 4, in the above-mentioned particle size range, show that the decomposition rate of limestone particles increased with decreasing particle size, the CO_2 evolution rate of limestone with larger particle size was relatively low, and the local CO_2 accumulation was larger, which easily led to the formation of wider, large cracks, while the CO_2 instantaneous generation rate of limestone with smaller particle size was larger, but the cumulative production was limited, and a sufficiently large pore pressure could not be generated, resulting in a large number of fine cracks on the particle surface.

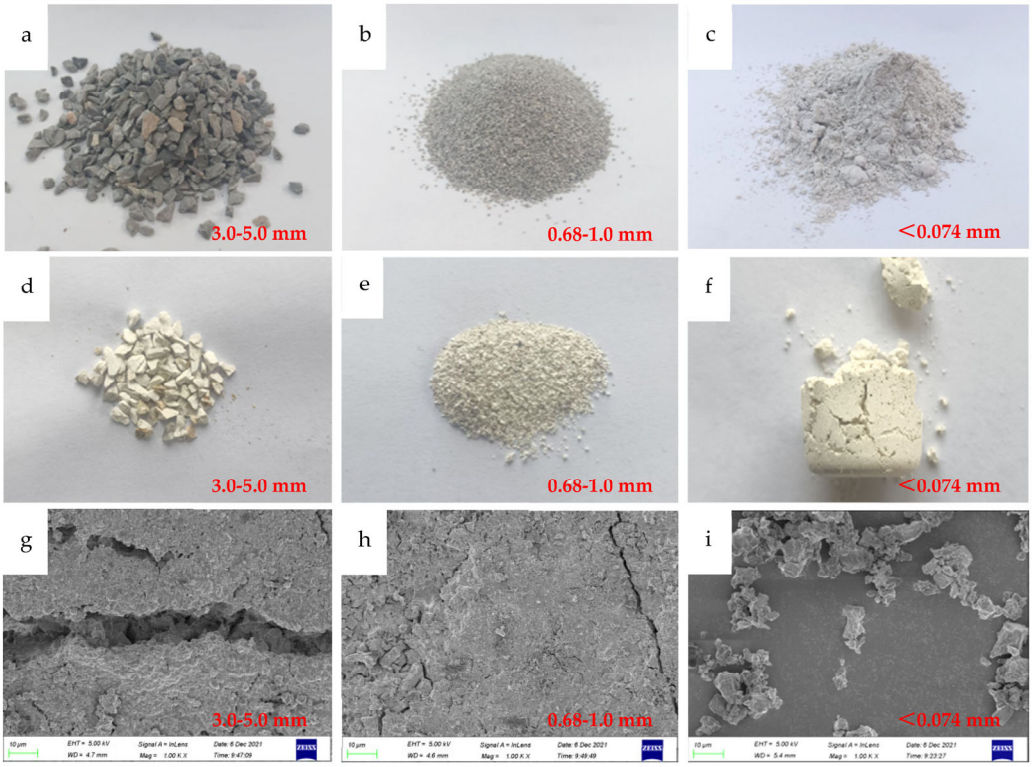

Figure 6. Comparison of limestone before and after calcination. Comparison of limestone before and after calcination. Original morphology of limestone particles before calcination for (**a**–**c**). Macroscopic morphology of limestone particles after calcination for (**d**–**f**). Microscopic morphology of the surface of limestone particles after calcination for (**g**–**i**).

No popping sound was heard during calcination of limestone particles with a particle size less than 0.074 mm. Additionally, no cracks were observed on the surface when viewed with a scanning electron microscope. However, since the limestone particles were too small and the inter-particle porosity was low, strong bonding occurred during calcination, and eventually lumpy lime was formed, as shown in Figure 6f,i.

Figure 7a–c shows the microstructure of three groups of limestone particles with a particle size range of 3.0–5.0 mm, 0.68–1.0 mm, and 0.074 mm after complete decomposition. It can be seen that all three groups of particle samples show the phenomenon of "overburning". The CaO grains started to fuse with each other at the grain boundaries, the holes were reduced, and a dense structure was formed.

In particular, the limestone particles with a particle size of 3.0–5.0 mm have a relatively low conversion degree, and the time required for complete decomposition is long, which means that CaO grains obtain sufficient driving force. The CaO grains continued to grow, and fuse in a large area, all pores disappeared, and the lime "burned to death" to form a denser overburned layer, as shown in Figure 7a.

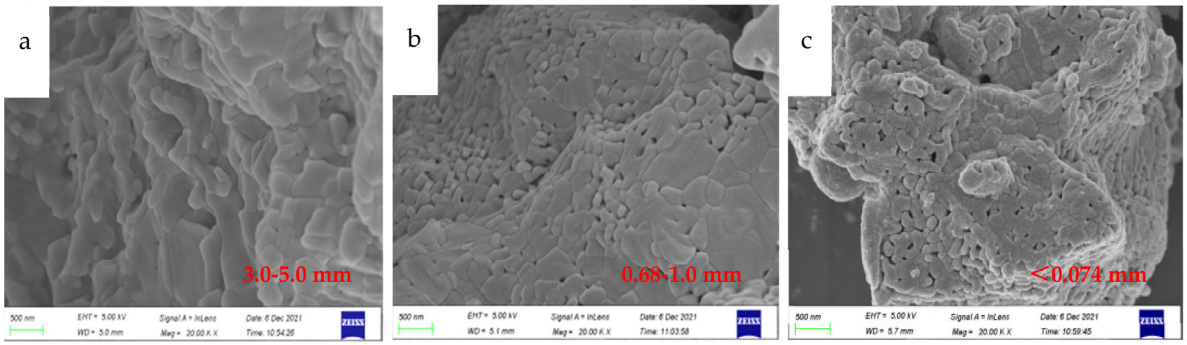

Figure 7. Microstructure of calcined limestone with different particle size. Microstructure of limestone particles with a particle size range of 3.0–5.0 mm for (**a**). Microstructure of limestone particles with a particle size range of 0.68–1.0 mm for (**b**). Microstructure of limestone particles with particle size less than 0.074 mm for (**c**).

Figure 8 shows the microscopic morphology comparison of three groups of limestone particles with particle size range of 3.0–5.0 mm, 0.68–1.0 mm, and 0.074 mm at 1623 K for 30 s (Figure 8a–c), 60 s (Figure 8d–f) and 100 s (Figure 8g–i). As shown in Figure 8a,d,g, the crystallo-chemical changes of limestone particles with a particle size of 3.0–5.0 mm occurred when calcined for 30 s, and a new phase nucleus of CaO was formed at some active points of the $CaCO_3$ surface. As the calcination time increased (60 s), the CaO grains increased and accumulated densely on the matrix. When the calcination time was 100 s, the local position began to show the structure of CaO grains and holes in a staggered arrangement, which was due to the escape of CO_2 from the $CaCO_3$ lattice structure and the transformation of $CaCO_3$ rhombic lattice into CaO cubic lattice, leaving a large number of pores.

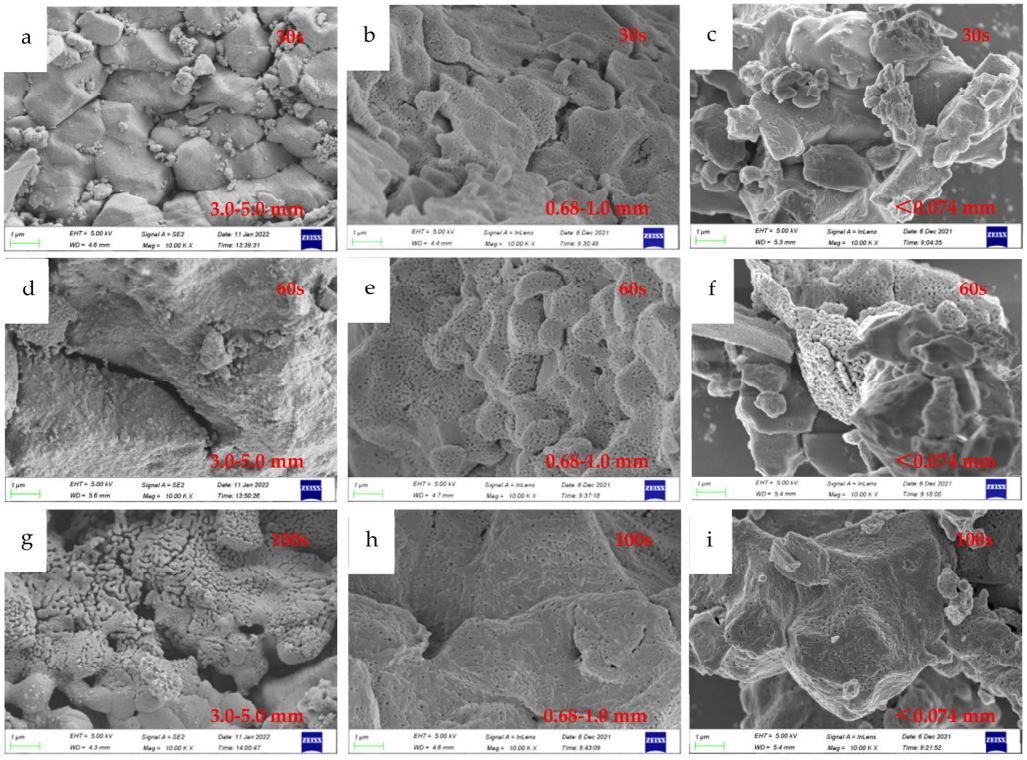

Figure 8. Microstructure of lime with different particle sizes calcined at different times. Microscopic morphology comparison of three groups of limestone particles at 1623 K for 30 s for (**a**–**c**). Microscopic morphology comparison of three groups of limestone particles at 1623 K for 60 s for (**d**–**f**). Microscopic morphology comparison of three groups of limestone particles at 1623 K for 100 s for (**g**–**i**).

As shown in Figure 8b,e,h, limestone particles with a particle size of 0.68–1.0 mm were already densely covered with initial CaO grains and micropores on the surface after only 30 s of calcination, and numerous small cracks were formed, which accelerated the escape of CO_2 gas and promoted the decomposition reaction. When the calcination time was 60 s, all the lime was laminar with cubic CaO grains arranged, the grain size was about 0.1 mm, and the crystal structure was not fully developed. When the calcination was continued to 100 s, the pores were much smaller and the CaO on the particles surface appeared "overburned".

As shown in Figure 8c,f,i, the calcination process of limestone particles with particle size less than 0.074 mm was more complicated due to their small size and easy bonding. With the prolongation of calcination time, there was a constant coexistence of primary CaO grains, a CaO grain-inclusion pore structure, and a dense CaO structure, which negatively affected the activity of lime.

3.4. Activity of Small-Sized Limestone Calcined Rapidly at High Temperature

The activity of lime represents its ability to participate in the steelmaking slagging reaction, and metallurgical lime generally must have an activity of 300 mL or more. High-activity lime can be rapidly slagged at the beginning of steelmaking to facilitate the dephosphorization reaction. The activity of seven groups of limestone particles with different particle sizes calcined at 1623 K was determined by the acid–base synthesis method.

Figure 9 shows the activity of limestone with different particle sizes when calcined for 30 s, 60 s, and 100 s, respectively. The different colors in the figure represent different numerical ranges of reaction activity, with blue representing the lowest reaction activity and red representing the highest reac-tion activity. For a calcination time of 30 s, the activity was less than 200 mL because the calcination time was too short, the conversion degree of limestone decomposition was low, and the amount of CaO produced was small. At calcination times of 60 s and 100 s, respectively, the activity increased and then decreased, with decreasing limestone particle size, which is consistent with the change in conversion degree in Figure 4. The maximum activity reached 370 mL when the limestone particle size was 0.68–1.0 mm and calcined for 60 s.

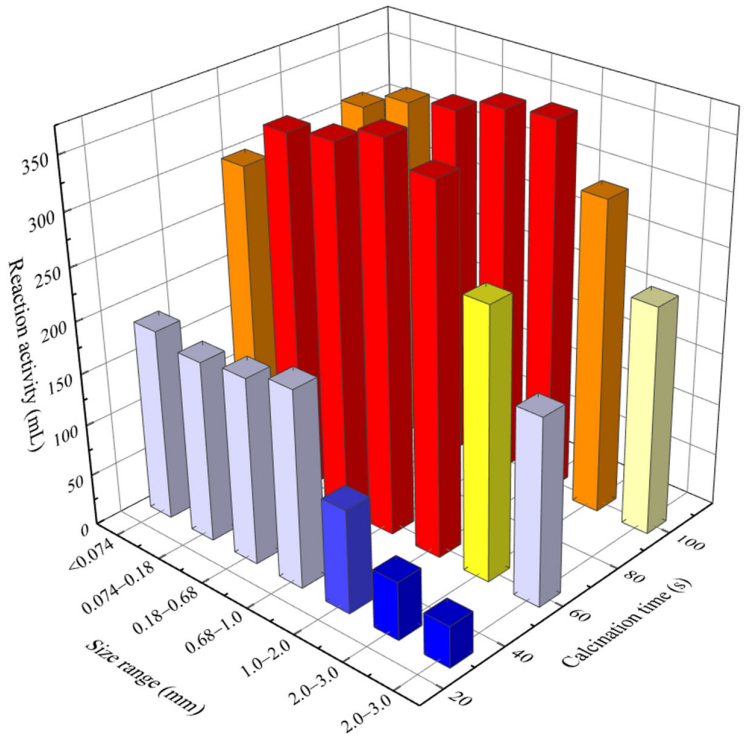

Figure 9. The activity of lime with different particle sizes calcined at different times.

Figure 10 shows the decomposition conversion degree and activity of 0.68–1.0 mm limestone particles calcined for different durations. As the duration of calcination increased, the limestone conversion degree increased, but the activity showed a trend that first increased and then decreased. The high temperature of 1623 K may have caused the limestone surface to calcine rapidly and produce highly active CaO, but due to the high calcination temperature, the CaO grains would rapidly develop and complete, and the activity would decrease. When the calcination time was 100 s, although the $CaCO_3$ was essentially completely decomposed and the unreacted layer disappeared, the thickness of the overburned layer also increased rapidly with increasing calcination time, the CaO grains near the surface of the particles grew rapidly, and the proportion of active lime decreased significantly compared with that from 60 s of calcination, resulting in a decrease in activity. This result indicates that the CaO produced during rapid calcination at steelmaking temperature was highly active, but also tended to overburn. In the middle stage of the decomposition reaction, the thickness of the reaction layer was relatively larger and the proportion of active lime was higher than in the initial stage and late stage of the reaction.

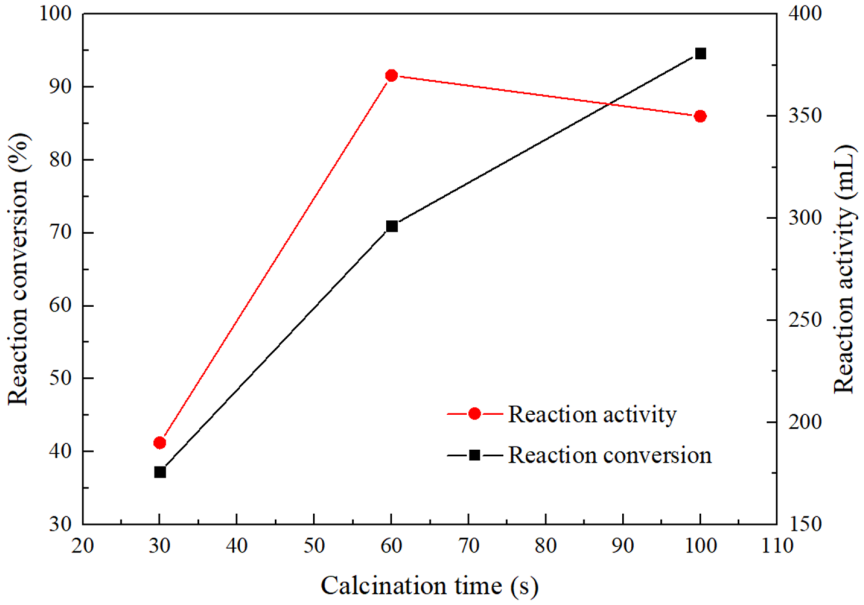

Figure 10. Conversion and activity of 0.68–1.0 mm limestone particles calcined at different times.

When limestone powder is injected into the converter to produce steel, the limestone has the property of slagging while it is calcined. The highly active CaO formed layer by layer during calcination of limestone chemically reacts with oxides such as (FeO) and (Fe_2O_3) in the slag, to be fully utilized in a timely manner.

Compared with limestone particle sizes of 0.18–0.68 mm and 0.68–1.0 mm, the conversion curves of the two essentially overlap, the changing pattern of activity at different times of calcination is the same, and the high activity of 355 mL can be achieved at 60 s of calcination. Therefore, it can be concluded that limestone particles with a particle size of 0.18 to 1.0 mm can be calcined rapidly and achieve high activity at 1623 K in the steelmaking process of injecting limestone powder into the converter, which provides certain theoretical guidance for the development of the new process and promotes the development of whole-process, low-carbon technology in the steel industry.

4. Conclusions

(1) When limestone with a small particle size is rapidly calcined at a high temperature, the duration of the decomposition reaction first decreases and then increases as the limestone particle size becomes smaller. The decomposition dynamics model is the shrinking sphere or cylinder model with phase boundary reaction, and the function

integral equation is $G(\alpha) = 1 - (1 - \alpha)^{1/n}$. When the particle size is 0.18–5.0 mm, the reaction order is n = 1/3, and when the particle size is less than 0.18 mm, the reaction order is n = 1/2.

(2) Limestone particles can form a structure in which CaO grains and micropores are arranged in a short amount of time in a high-temperature environment, but as the calcination time increases, the phenomenon of "overburning" occurs. Limestone particles with a particle size of 0.68–1.0 mm were calcined for 60 s to obtain the typical microstructure of active lime.

(3) During high-temperature calcination of limestone particles at 1623 K to complete decomposition, the activity shows a change rule of first increasing and then decreasing. At high temperature, limestone can be rapidly calcined to form highly active CaO, but in the later stage of the reaction, the thickness of the overburned layer rapidly increases, the proportion of active lime decreases and the activity decreases.

(4) Limestone particles with a particle size of 0.18–1.0 mm are able to complete rapid calcination at 1623 K and achieve high activity above 350 mL, which is the preferred limestone particle size range for the steelmaking process in which limestone powder is injected into the converter.

However, the movement and distribution of limestone particles in the high-temperature molten pool should also be comprehensively studied when determining the particle size of limestone in this process, which will be studied through numerical simulation and physical simulation in the follow-up work.

Author Contributions: K.Z. and C.L. conceived and designed the study; H.S. and Y.Z. performed the calculation; H.S. and K.Z. conducted the experiment; S.W. and C.L. analyzed the experimental data; and K.Z. and C.L. wrote the paper. All authors have read and agreed to the published version of the manuscript.

Funding: This research was funded by the National Natural Science Foundation of China, grant number 52004097; the Innovation Funding Project for Graduate Students of Hebei Province, grant number CXZZBS2022113; and the Basic Scientific Research Fee Project of North China University of Science and Technology, grant number JQN2021003.

Data Availability Statement: Not applicable.

Acknowledgments: The authors gratefully acknowledge the support of the Tangshan Key Laboratory of Special Metallurgy and Material Manufacture.

Conflicts of Interest: The authors declare no conflict of interest.

References

1. Li, H.; Qu, Y. *A Method for Slag-Making Steelmaking with Limestone Instead of Lime in Oxygen Top-Blown Converter*; Metallurgical Industry Press: Beijing, China, 2009.
2. Du, Y.T. Research on Low-Phosphorus Steel Smelting Process Using Limestone in Converter. Ph.D. Thesis, University of Science and Technology Beijing, Beijing, China, 15 June 2017.
3. Liu, H.Z. Research on energy-saving and emission-reduction measures for replacing lime with limestone in steel-making raw materials. *China Steel Focus* **2020**, *17*, 160–161.
4. Li, H.; Guo, L.F.; Li, Z.Q.; Song, W.C.; Li, Y.Q. Research of low-carbon mode and on limestone addition instead of lime in the BOF steelmaking. *J. Iron Steel Res. Int.* **2010**, *172*, 23–28.
5. Jose, M.V. On the negative activation energy for limestone calcination at high temperatures nearby equilibrium. *Chem. Eng. Sci.* **2015**, *132*, 169–177.
6. Wang, X.Y.; Li, J.L.; Xue, Z.L. Reactivity and grain size of lime calcined rapidly at high temperature. *Bull. Chin. Ceram. Soc.* **2016**, *35*, 374–379+391.
7. Xue, Z.L.; Ke, C.; Liu, Q.; Li, P.; Yang, S.B. Study on the reactivity of lime fast calcined at high temperature. *Steelmaking* **2011**, *27*, 37–40.
8. Moropoulou, A.; Bakolas, A.; Aggelakopoulou, E. The effects of limestone characteristics and calcination temperature on the reactivity of quicklime. *Cem. Concr. Res.* **2001**, *31*, 633–639. [CrossRef]
9. Houngaloune, S.; Ariffin, K.S.; Hussin, H.B.; Watanabe, K.B.; Nhinxay, V.C. The effects of limestone characteristic, granulation and calcination temperature to the reactivity of quicklime. *Malays. J. Microsc.* **2010**, *6*, 53–57.
10. Kili, Z. Effects of limestone characteristic properties and calcination temperature on lime quality. *Asian J. Chem.* **2006**, *18*, 655–666.

11. Hu, B.; Xue, Z.L.; Bai, S.; Li, J.; Li, J.L.; Cai, J.L. Kinetics study on decomposition reaction of limestone under ultra-high temperature. *Steelmaking* **2017**, *33*, 56–61.
12. Ghiasi, M.; Abdollahy, M.; Khalesi, M. Investigating the kinetics, mechanism, and activation energy of limestone calcination using isothermal analysis methods. *Mining Metall. Explor.* **2021**, *38*, 129–140. [CrossRef]
13. Cai, J.L.; Xue, Z.L.; Xiong, T.Y.; Xie, Y.C.; Hu, B.; Li, J.L. Study on the physico-chemical properties and microstructure of lime rapidly calcined at high temperature. *Steelmaking* **2017**, *33*, 43–48.
14. Li, C.X.; Wang, S.H.; Zhao, D.G.; Li, H.; Xue, Y.K. Effect of microscopic morphology of limestone on its physical and chemical properties after calcining. *Mult. Util. Mineral Res.* **2020**, *1*, 184–187.
15. Wang, L.Y.; Xue, Z.L.; Cai, J.L.; Hu, B. Relationship between microstructure and properties of limestone calcined rapidly at high temperatures. *Trans. Indian Inst. Met.* **2019**, *72*, 3215–3222. [CrossRef]
16. Hu, R.Z.; Shi, Q.Z. *Thermal Analysis of the Kinetics*; Science Press: Beijing, China, 2008.
17. Huang, X.H. *Principles of Steel Metallurgy*, 4th ed.; Metallurgical Industry Press: Beijing, China, 2013.
18. Guo, H.J. *Theory and Process of Active Lime Production*; Chemical Industry Press: Beijing, China, 2014.
19. Wang, L.Y. A Dissertation Submitted in Partial Fulfillment of the Requirements for the Degree of Doctor of Philosophy in Engineering. Ph.D. Thesis, Wuhan University of Science and Technology, Wuhan, China, 20 June 2020.
20. Cui, Z.Q.; Qin, Y.C. *Metallography and Heat Treatment*, 2nd ed.; Machinery Industry Press: Beijing, China, 2007.
21. Fu, Y.F.; Huang, Y.L.; Pan, Z.S.; Tang, C.A. Literature review of study on mechanism of explosive spalling in concrete at elevated temperatures. *J. Build. Mater.* **2006**, *9*, 323–329.
22. Hu, B.; Li, J.L.; Li, J.; Bai, S.; Cai, J.L.; Xue, Z.L. The explosion behavior of limestone particles during calcination at steelmaking temperature. *Steelmaking* **2017**, *33*, 34–38.